

Article

Tuning the Gas Separation Performances of Smectic Liquid Crystalline Polymer Membranes by Molecular Engineering

Joey Kloos ¹, Menno Houben ¹, Johan Lub ², Kitty Nijmeijer ¹, Albert P. H. J. Schenning ²
and Zandrie Borneman ^{1,*}

¹ Membrane Materials and Processes, Department of Chemical Engineering and Chemistry, Eindhoven University of Technology, P.O. Box 513, 5600 MB Eindhoven, The Netherlands

² Stimuli-Responsive Functional Materials and Devices, Department of Chemical Engineering and Chemistry, Eindhoven University of Technology, P.O. Box 513, 5600 MB Eindhoven, The Netherlands

* Correspondence: z.borneman@tue.nl

Abstract: The effect of layer spacing and halogenation on the gas separation performances of free-standing smectic LC polymer membranes is being investigated by molecular engineering. LC membranes with various layer spacings and halogenated LCs were fabricated while having a planar aligned smectic morphology. Single permeation and sorption data show a correlation between gas diffusion and layer spacing, which results in increasing gas permeabilities with increasing layer spacing while the ideal gas selectivity of He over CO₂ or He over N₂ decreases. The calculated diffusion coefficients show a 6-fold increase when going from membranes with a layer spacing of 31.9 Å to membranes with a layer spacing of 45.2 Å, demonstrating that the layer spacing in smectic LC membranes mainly affects the diffusion of gasses rather than their solubility. A comparison of gas sorption and permeation performances of smectic LC membranes with and without halogenated LCs shows only a limited effect of LC halogenation by a slight increase in both solubility and diffusion coefficients for the membranes with halogenated LCs, resulting in a slightly higher gas permeation and increased ideal gas selectivities towards CO₂. These results show that layer spacing plays an important role in the gas separation performances of smectic LC polymer membranes.

Keywords: liquid crystal; polymer membranes; gas separation; layer spacing



Citation: Kloos, J.; Houben, M.; Lub, J.; Nijmeijer, K.; Schenning, A.P.H.J.; Borneman, Z. Tuning the Gas Separation Performances of Smectic Liquid Crystalline Polymer Membranes by Molecular Engineering. *Membranes* **2022**, *12*, 805. <https://doi.org/10.3390/membranes12080805>

Academic Editors: David Alique and David Martinez-Diaz

Received: 27 July 2022

Accepted: 18 August 2022

Published: 20 August 2022

Publisher's Note: MDPI stays neutral with regard to jurisdictional claims in published maps and institutional affiliations.



Copyright: © 2022 by the authors. Licensee MDPI, Basel, Switzerland. This article is an open access article distributed under the terms and conditions of the Creative Commons Attribution (CC BY) license (<https://creativecommons.org/licenses/by/4.0/>).

1. Introduction

The vast majority of our energy production is generated by the combustion of fossil fuels (e.g., coal and natural gas), which results in enormous amounts of greenhouse gasses such as CO₂ and CH₄ being released into the atmosphere, leading to a rise in the average temperature of the Earth's atmosphere [1,2]. For a sustainable future, greenhouse gas emissions must be reduced, which makes separations such as CO₂/CH₄ and CO₂/N₂ crucial and relevant [3–6]. Polymeric membrane processes are, among other technologies, used for gas separation processes because of their low operating costs, high energy efficiency and easy scalability compared to other separation technologies [2,7–9]. However, most polymeric membranes used for gas separation are not ordered and aligned at the mesoscopic level, which affects the gas permeability and selectivity [4,8,10–12]. Using materials with self-assembly properties to obtain nanostructured polymer membranes provides additional parameters, such as control over the molecular order and alignment of the membrane building blocks, to tailor the gas separation properties. However, the effect of molecular order on the gas separation performance of such nanostructured materials has been rarely reported.

Liquid crystal (LC) molecules can self-assemble into various nanometer structures, which, depending on the positional order of the LC monomers and the fabrication process, can differ in molecular order and orientation. A frequently used fabrication method is to induce self-assembly of reactive LC monomers inside a cell with spacer beads to tune the

membrane thickness and alignment layers to control the molecular orientation. Subsequent crosslinking of the LC monomers to fixate the nanostructures is necessary to provide sufficient mechanical strength to obtain robust free-standing LC polymer membranes. So far, LC polymer membranes have mainly been investigated for water separations [13–24], but hardly for gas separations [25–27]. Studies show the importance of molecular order and orientation in LC polymer membranes, see, for example, our previous work [26]. Here, highly ordered smectic C (lamellar nanostructured) membranes have lower gas permeabilities but selectivity towards He and CO₂ over N₂ increases tremendously compared to the membranes without molecular order (see Figure 1b for an artist's impression of a top view of an LC membrane with a smectic C morphology) [26]. Moreover, the highly ordered smectic C membranes with lamellar structures parallel to the permeation direction (planar alignment) exhibit higher gas permeations but lower selectivities compared to membranes with lamellar structures perpendicular to the permeation direction (homeotropic alignment). However, so far, the role of the dimensions of the nanostructures in the membranes on the gas separation properties has not been reported yet [28]. Moreover, incorporating halogen atoms such as chlorine or fluorine is known to enhance CO₂ permeability and selectivity by affecting both gas solubility and diffusion [29–32] and in addition, it also provides a more detailed insight into the gas transport in smectic LC polymer membranes.

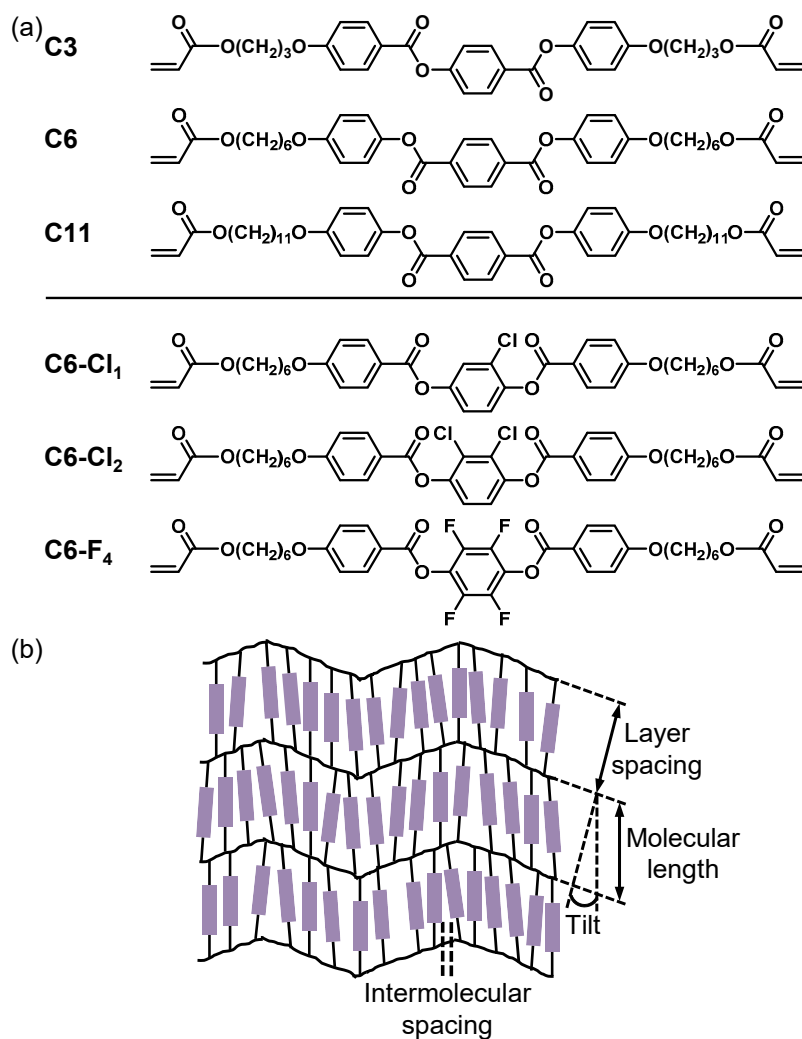


Figure 1. (a) Chemical structures of the LCs used in this research. (b) Artist impression of a top view of the planar aligned smectic C membranes, which shows the layer spacing, molecular length, intermolecular spacing and tilt angle of the LC molecules. The purple rods represent the aromatic cores of the LCs.

Here, we investigate the effects of the layer spacing and halogenation on the gas separation performance of free-standing planar aligned smectic LC polymer membranes for gas separations of He, CO₂ and N₂. Various smectic LC membranes are fabricated and characterized by consisting of either LCs with the same functional group but different alkyl spacer length or mixtures of two LCs with the same molecular length but containing different halogenated LCs (see Figure 1a for the LCs used in this research). The effect of layer spacing on the gas separation performances of smectic LC membranes is shown by measuring single gas sorption and permeation of various gasses through membranes with various layer spacings. The effect of halogenation on the gas separation properties of smectic LC membranes is investigated by measuring the single gas sorption and permeation performances of membranes that contain different halogenated LCs.

2. Materials and Methods

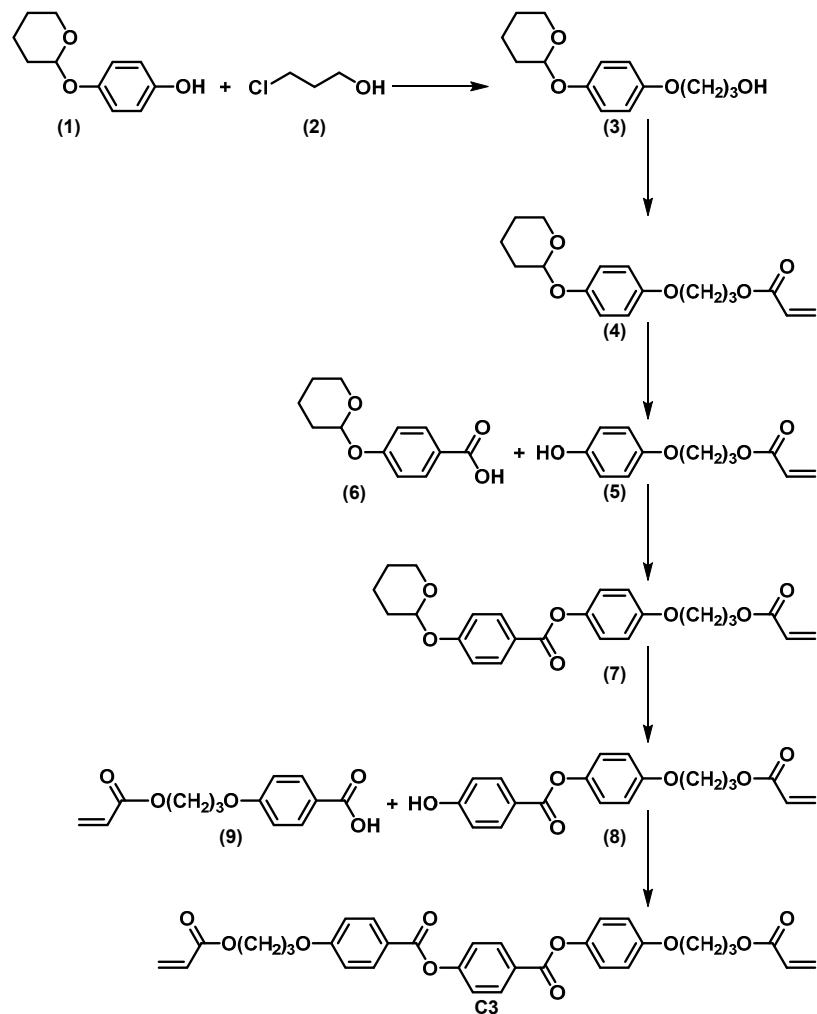
2.1. Chemicals

The LC diacrylates 1,4-di-(4-(6-acryloyloxyhexyloxy)phenyl)terephthalate (**C6**) [33] and di-4-(11-acryloyloxyundecyloxy)phenyl terephthalate (**C11**) [26] were prepared as described in previous publications. The 2,3,5,6-tetrafluoro-4-(4-(6-acryloyloxyhexyloxy)benzoyloxy)phenyl 4-(6-acryloyloxyhexyloxy)benzoate (**C6-F₄**) was prepared as described in the literature [34]. The synthesis of 4-(3-acryloyloxypropyloxy)phenyl 4-(4-(3-acryloyloxypropyloxy)benzoyloxy)benzoate (**C3**) is outlined in Scheme 1. (3-(acryloyloxy)propoxy)benzoic acid (**9**) was obtained from Synthon. The 4-((tetrahydro-2H-pyran-2-yl)oxy)phenol (**1**) and 4-((tetrahydro-2H-pyran-2-yl)oxy)benzoic acid (**6**) were both made according to a literature procedure [33]. The syntheses of 2,3-dichloro-1,4-phenylene bis(4-((6-(acryloyloxy)hexyl)oxy)benzoate) (**C6-Cl₂**) and 2-chloro-1,4-phenylene bis(4-((6-(acryloyloxy)hexyl)oxy)benzoate) (**C6-Cl₁**) are outlined in Scheme 2. The 4-(6-acryloyloxyhexyloxy)benzoic acid (**10**) was obtained from synthon and 2,3-dichlorohydroquinone (**12a**) was made according to a literature procedure [35].

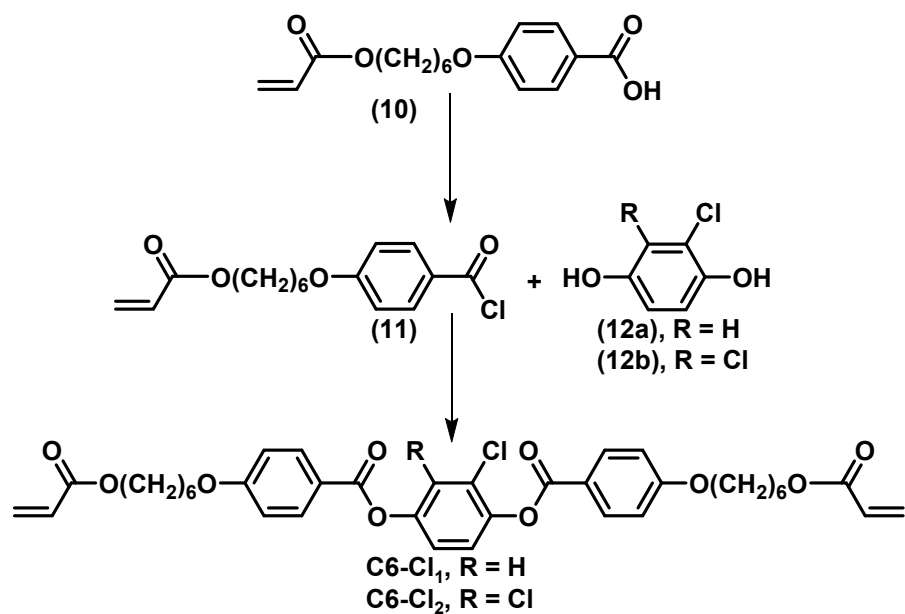
All other chemicals used for the synthesis of the LC monomers were obtained from Sigma-Aldrich (Zwijndrecht, the Netherlands). The synthetic preparations of the molecules in Schemes 1 and 2 are described in the supporting information. Irgacure 819 was supplied by Ciba. t-Butyl-hydroquinone was purchased from Merck Life Science (Amsterdam, the Netherlands). For permeation and sorption measurements, the gasses He (5.0 grade), CO₂ (4.5 grade) and N₂ (5.0 grade) were obtained from Linde Gas (Schiedam, the Netherlands). All reagents were used as received without further purification.

2.2. Membrane Preparation

LC mixtures with 0.5 wt% Irgacure 819 (photoinitiator) and 0.1 wt% t-butyl-hydroquinone (inhibitor) were prepared by dissolving the compounds in a minimum amount of chloroform and subsequently evaporating the solvent (LCs and fabrication conditions are displayed in Table 1, see Figure 1a for chemical structures). Planar aligned smectic C membranes were fabricated by processing the LC mixtures in the smectic phase by capillary suction between two accurately 20 μm spaced glass plates. The glass plates were cleaned before use with isopropanol in an ultrasonic bath for 30 min, dried with N₂ and treated with UV ozone for 30 min. To obtain planar alignment, the glass plates were functionalized with a rubbed polyimide layer (Optimer AL 1254; JSR Corporation, Toyo, Japan). Glass cells were prepared by gluing two functionalized glass plates together with glue that contained 20 μm glass spacer beads. The filled LC cells were placed inside a temperature-controlled N₂ box, in which the cells were cooled from the isotropic phase to the smectic phase using a cooling rate of 3 °C/min and subsequently polymerized by exposing the samples for 10 min to an unfiltered spectrum of a collimated EXFO Omnicure S2000 UV lamp (Excelitas Technologies, Germany) with a light intensity of 20 mW/cm² in the range of 320–390 nm. Free-standing membranes were obtained by opening the glass cells in hot water (80 °C).



Scheme 1. Synthetic route to 4-(3-acryloyloxypropoxy)phenyl 4-(4-(3- acryloyloxypropoxy)benzoyloxy) benzoate (C3).



Scheme 2. Synthetic routes to 2-chloro-1,4-phenylene bis(4-((6-(acryloyloxy)hexyl)oxy)benzoate) (C6-Cl₁) and 2,3-dichloro-1,4-phenylene bis(4-((6-(acryloyloxy)hexyl)oxy)benzoate) (C6-Cl₂).

Table 1. Fabrication conditions for LC membranes with various layer spacings and LC membranes with various halogenated LCs.

Compound/ Mixtures	Isotropic Temperature [°C]	Polymerization Temperature [°C]	Cooling Rate [°C/min]
C3	180	100	3
C6	155	130	3
C11	140	122	3
C6 with 30 wt% C6-Cl ₁	140	110	3
C6 with 30 wt% C6-Cl ₂	145	115	3
C6 with 25 wt% C6-F ₄	140	108	3

2.3. Characterization

Nuclear magnetic resonance (NMR) spectra were recorded on a 400 MHz Bruker Avance III HD spectrometer in deuterated chloroform with tetramethyl silane (TMS) as the internal standard.

Matrix-assisted laser desorption/ionization time-of-flight mass spectrometry (MALDI-TOF MS) was performed on a Bruker Autoflex Speed MALDI-MS instrument using DCTB (2-[(2E)-3-(4-tert-butylphenyl)-2-methylprop-2-enylidene] malononitril) as matrix.

Attenuated total reflection Fourier transform infrared spectroscopy (ATR FT-IR) spectra were recorded at room temperature on a Varian-Cary 3100 FT-IR spectrometer (Vlissingen, the Netherlands) equipped with a golden gate attenuated total reflectance (ATR) sampling accessory. Scans were taken over a range of 4000–650 cm⁻¹ with a spectral resolution of 4 cm⁻¹ and 50 scans per spectrum.

Polarizing optical microscopy (POM) was performed using a Leica DM 2700M optical microscope equipped with two polarizers that were operated either crossed or parallel with the sample in between a Linkam hot-stage THMS600 with a Linkam TMS94 controller and a Leica DFC420 C camera.

Differential scanning calorimetry (DSC) measurements were recorded in hermetic T-zero aluminum sample pans using a TA Instruments Q2000 DSC equipped with a cooling accessory. The DSC measurements were performed with three cycles of heating and cooling at a rate of 3 °C/min with an isothermal equilibration of 3 min after each heating or cooling ramp.

Medium- and wide-angle X-ray scattering (MAXS/WAXS) measurements were recorded on a GaneshaLab instrument (Lyngby, Denmark) equipped with a Genix-Cu ultralow divergence source producing X-ray photons of wavelength 1.54 Å and a flux of 108 photons per second. Diffraction patterns were collected on a Pilatus 300 K silicon pixel detector with 487 × 619 pixels of 172 μm².

2.4. Gas Sorption

Gas sorption was measured with a Rubotherm series IsoSORP[®] sorption instrument (Bochum, Germany) to determine the CO₂ solubility coefficient of all membranes. Before each measurement, the sample was degassed for 5 h by applying a vacuum to the measuring cell followed by a buoyancy measurement with helium to determine the initial sample weight and volume of the sample. Here it was assumed that the solubility of helium is negligible. Gas sorption of CO₂ was measured at 6 bar and 40 °C (with an equilibrium time of 3 h). The measured sorbed weight was corrected for the buoyancy effect according to Equation (1).

$$m_{\text{corrected}} = m_{\text{measured}} + \rho_{\text{gas}} \cdot V_{\text{sample}} \quad (1)$$

In Equation (1) $m_{\text{corrected}}$ is the corrected weight (g), m_{measured} is the measured weight (g), ρ_{gas} is the density of the measuring gas (g/cm³) and V_{sample} is the sample volume (cm³). The concentration of CO₂ was calculated using Equation (2).

$$C_{\text{CO}_2} = \frac{m_{\text{CO}_2} \cdot \rho_s}{m_0 \cdot \rho_{\text{CO}_2} (\text{STP})} \quad (2)$$

In Equation (2) C_{CO_2} is the concentration of CO_2 in the membrane (cm^3 (STP)/ cm^3 polymer), m_{CO_2} is the buoyancy corrected mass of CO_2 in the polymer (g), ρ_s is the density of the membrane (g/cm^3), m_0 is the initial mass of the sample measured at vacuum (g) and ρ_{CO_2} is the density of CO_2 gas at standard temperature and pressure (STP) (STP = 273.15 K and 1.013 bar) (g/cm^3). The CO_2 solubility coefficient was calculated using Equation (3).

$$S_{\text{CO}_2} = \frac{C_{\text{CO}_2}}{P} \quad (3)$$

In Equation (3) S_{CO_2} is the gas solubility of CO_2 (cm^3 STP/($\text{cm}^3 \cdot \text{cmHg}$)), C_{CO_2} is the concentration of CO_2 in the membrane (cm^3 (STP)/ cm^3 polymer) and P is the pressure (cmHg).

2.5. Single Gas Membrane Performances

Single gas permeation measurements of He, CO_2 and N_2 were performed in a custom-built permeation setup. The flat sheet membranes supported by a Whatman[®] filter paper (Grade 50 with a pore size of 2.7 μm) to prevent possible pressure-induced punctures, were placed in a stainless-steel cell with a permeation area of 2.1 cm^2 and the membrane cell was subsequently put in an oven (Convergence Inspector Hephaistos, Enschede, the Netherlands) to control the temperature. Single gas permeabilities were determined from the steady-state pressure increase in time in a calibrated volume at the permeate side of the membrane. The single gas permeabilities were calculated using Equation (4) at 40 °C for two different samples by measuring the permeate pressure increase over time in a calibrated volume with a feed pressure of 6 bar against a vacuum at the permeate side.

$$P_i = \frac{\Delta P_{\text{permeate}} \cdot V_c \cdot V_m \cdot L \cdot 10^{10}}{\Delta t \cdot R \cdot T \cdot A \cdot \Delta P} \quad (4)$$

In Equation (4) P_i is the permeability of gas species i (Barrer), $\Delta P_{\text{permeate}}$ is the increase in permeate pressure (Pa) per time interval Δt (s), V_c is the calibrated permeate volume (m^3), V_m is the molar volume at STP (cm^3/mol), L is the membrane thickness (cm), R is the gas constant ($\text{J}/\text{K} \cdot \text{mol}$), T is the permeate temperature (K), A is the membrane area (cm^2) and ΔP is the transmembrane pressure (cmHg). The membrane thickness in Equation (4) was determined by taking the average thickness of 7 spots that were measured over the entire membrane area with a micrometer. Before the permeation measurements, the membranes were conditioned overnight (for 12 h) at 6 bar at the feed side with the gas to be measured and vacuum at the permeation side. Subsequently, the permeation of each gas was measured in triplicate on the same membrane. The order of the measured gasses was kept constant for all membranes (He, N_2 and CO_2) since CO_2 could induce swelling of the membrane. The ideal selectivity ($\alpha_{i/j}$) was calculated using the single gas permeabilities as shown in Equation (5), where P_i is the permeability of gas species i (Barrer) and P_j is the permeability of gas species j (Barrer).

$$\alpha_{i/j} = \frac{P_i}{P_j} \quad (5)$$

The CO_2 diffusion coefficients of all membranes were calculated by using Equation (6).

$$D = \frac{P}{S} \quad (6)$$

In Equation (6), D is the diffusion coefficient (cm^2/s), P the permeability (Barrer) and S the solubility coefficient (cm^3 STP/($\text{cm}^3 \cdot \text{cmHg}$)).

3. Results and Discussion

3.1. Preparation and Characterization of the Liquid Crystalline Molecules and Mixtures

The effect of layer spacing on the gas separation performance of planar aligned smectic LC polymer membranes was studied by varying the length of the alkyl spacers in the

LC monomers (**C3**, **C6** and **C11** in Figure 1a). The role of the chemical composition was investigated by incorporating bulky halogen groups such as chlorine or fluorine on the rigid LC core, which are known to enhance CO₂ permeability and selectivity (**C6-Cl₁**, **C6-Cl₂** and **C6-F₄** in Figure 1a) [29–32]. The LC monomers **C6**, **C11** and **C6-F₄** were synthesized and characterized as described in the literature [26,33,34], while **C3**, **C6-Cl₁** and **C6-Cl₂** were synthesized for the first time (see Schemes 1 and 2 for synthesis schemes). Characterization by ¹H and ¹³C nuclear magnetic resonance (NMR) and mass spectroscopy (MALDI-TOF MS) confirmed the successful synthesis of all molecules. The phase transitions of all molecules were determined with differential scanning calorimetry (DSC) and polarizing optical microscopy (POM). These results are shown in Table 2 (see Figures S1–S6 for DSC and POM).

Table 2. Phase transitions of the synthesized LCs.

Compound	Isotropic [°C]	Nematic [°C]	Smectic [°C]
C3	>174	174–113	113–48
C6	>146	146–142	142–113
C11	>132	132–131	131–116
C6-Cl₁	>110	110–99	-
C6-Cl₂	>139	139–104	-
C6-F₄	>109	109–104	-

DSC and POM (Table 2) show that the **C3**, **C6** and **C11** monomers exhibit nematic and smectic mesophases but at different temperatures. **C11** has the longest flexible alkyl spacer of all synthesized LCs, resulting in the lowest phase transitions. Contrary, **C3** has the shortest alkyl spacer with less flexibility, which leads to the highest phase transitions of all LCs [36]. Only LC mixtures that exhibit a smectic mesophase were used to prepare membranes. Because the pure **C6-Cl₁**, **C6-Cl₂** and **C6-F₄** monomers only exhibit a nematic mesophase, LC mixtures consisting of **C6** with **C6-Cl₁**, **C6-Cl₂** and **C6-F₄** were prepared and characterized with DSC and POM (see Figures S7–S9 for DSC and POM and Table S1 for phase transition values). Compositions containing more than 30 wt% **C6-Cl₁** or **C6-Cl₂** and 25 wt% **C6-F₄** did not exhibit a smectic mesophase and were therefore not used in this study. Hence, LC mixtures consisting of **C6** with respectively 30 wt% **C6-Cl₁** or **C6-Cl₂** and 25 wt% **C6-F₄** were used to prepare membranes to study the effect of halogenation on the gas separation performances of smectic LC membranes.

3.2. Preparation and Characterization of Liquid Crystalline Membranes

The LCs were mixed with a photoinitiator to fabricate LC membranes by photopolymerization. Planar-aligned smectic LC membranes were prepared by incorporating the LC mixtures in glass cells with alignment layers to control the orientation of the LCs. After heat treatment, the LC mixtures were photopolymerized in the smectic mesophase to fixate the lamellar morphology. Free-standing LC membranes were obtained by opening the glass cells (see Figure 1b for an artist's impression of a top view of a planar-aligned smectic C membrane). FT-IR spectra before and after polymerization showed full conversion of the acrylate moieties (Figure S10).

The alignment and morphology of the membranes were investigated with POM (Figure S11) and showed the planar alignment of all membranes with dark images under parallel conditions and bright images under 45° tilt. Wide-angle X-ray scattering (WAXS) and medium-angle X-ray scattering (MAXS) were measured to further study the morphology and alignment of the membranes (Figure 2).

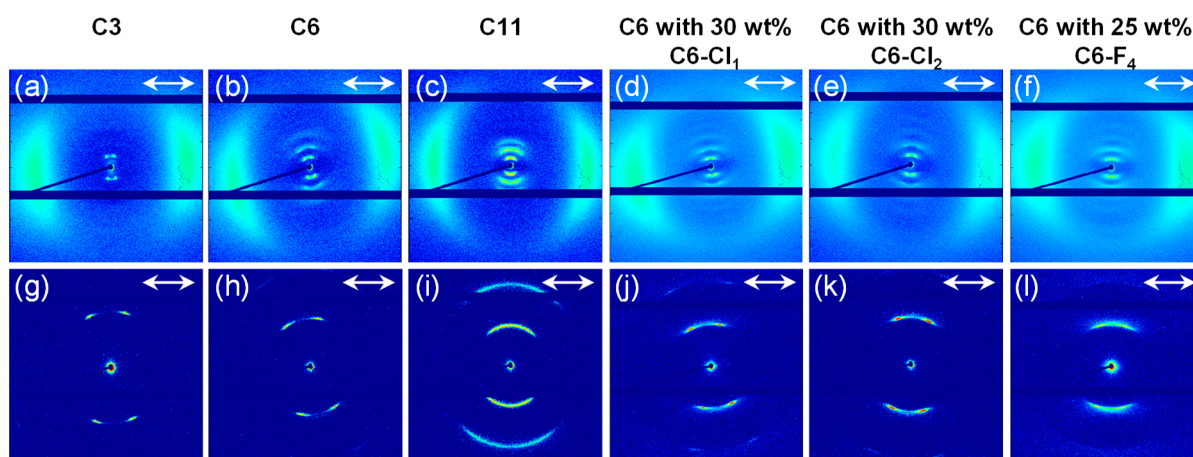


Figure 2. WAXS (top row) and MAXS (bottom row) spectra of LC membranes consisting of LCs with various alkyl spacer lengths and various halogenated LCs. (a,g) C3, (b,h) C6, (c,i) C11, (d,j) C6 with 30 wt% C6-Cl₁, (e,k) C6 with 30 wt% C6-Cl₂, (f,l) C6 with 25 wt% C6-F₄. The single arrow shows the alignment direction.

The 2D WAXS and MAXS spectra in Figure 2 show for all membrane diffraction lobes/spots, indicating that all molecules are aligned. The MAXS spectra of the C3 (Figure 2g), C6 (Figure 2h), C6 with 30 wt% C6-Cl₁ (Figure 2j) and C6 with 30 wt% C6-Cl₂ (Figure 2k) membranes show four diffraction spots parallel to the alignment direction, which corresponds to an ordered smectic C morphology. The MAXS spectra of the C11 membranes (Figure 2i) and the C6 membranes with 25 wt% C6-F₄ (Figure 2l) show diffraction lobes instead of spots, which is characteristic of the morphology between smectic A and smectic C [33]. The more smectic A character of the C11 membranes compared to the C6 and C3 membranes likely arises due to the increased flexibility of the longer alkyl spacer in the C11 membranes, leading to less stress in the lamellar layers and resulting in a more smectic A morphology. Besides the membrane morphology also the tilt angle, layer spacing and intermolecular spacing were determined from the WAXS and MAXS spectra (Table 3).

Table 3. Morphology, tilt angle, layer spacing and intermolecular spacing of the fabricated LC membranes.

Membranes	Morphology	Tilt Angle [°]	Layer Spacing [Å]	Intermolecular Spacing [Å]
C3	SmC	21	31.9	4.6
C6	SmC	20	36.8	4.6
C11	SmA/C	18	45.2	4.6
C6 with 30 wt% C6-Cl ₁	SmC	20	37.4	4.5
C6 with 30 wt% C6-Cl ₂	SmC	22	37.5	4.6
C6 with 25 wt% C6-F ₄	SmA/C	20	38.1	4.5

Table 3 shows that the tilt angle of the smectic structures is similar for all membranes (varying between 18° and 22°) and is not affected by either extending the alkyl spacer in the LC monomers or by incorporating halogen groups into the LC core. However, the layer spacing, which corresponds to the distance between two layers, is found to be highly dependent on the length of the alkyl spacer in the LC membranes. The determined layer spacing is equal to 31.9 Å for the C3, 36.8 Å for the C6 and 45.2 Å for the C11 membranes, which is in close agreement with the theoretical extended molecular length of the LC monomers (34.0 Å for C3, 40.0 Å for C6 and 49.9 Å for C11). The small difference between the experimentally measured and theoretical layer spacing can be explained by the fact that the flexible alkyl spacers in the molecules are likely folded, leading to slightly lower layer spacing values. Surprisingly, the C6 membranes that contain halogenated LCs show slightly higher layer spacing values compared to the C6 membranes without halogenated

LCs. The layer spacing further increases with increasing halogen content, leading to the highest layer spacing for the C6 membranes with 25 wt% C6-F₄ (38.1 Å compared to 36.8 Å for the C6 membranes). Here, the bulky halogen groups can lead to more elongated alkyl chains, which results in slightly higher layer spacing values. The intermolecular spacing that corresponds to the intermolecular stacking of the LC molecules is not affected by the halogen groups and was found to be similar for all membranes (varying between 4.5 and 4.6 Å). The above confirms a planar alignment and smectic morphology for all fabricated LC membranes.

3.3. Effect of Layer Spacing on Single Gas Performances

The effect of the layer spacing on the gas permeation properties of smectic LC membranes was investigated by measuring the single gas permeation of He, CO₂ and N₂ at 40 °C in smectic LC membranes with various layer spacings. Permeation data and ideal gas selectivities of He/N₂, CO₂/N₂ and He/CO₂ are shown in Figure 3 (see Tables S2 and S3 for all permeation and ideal selectivity values). To show the effect of the layer spacing in more detail, the permeation data were also plotted against the layer spacing of the respective membranes (Figure 3c).

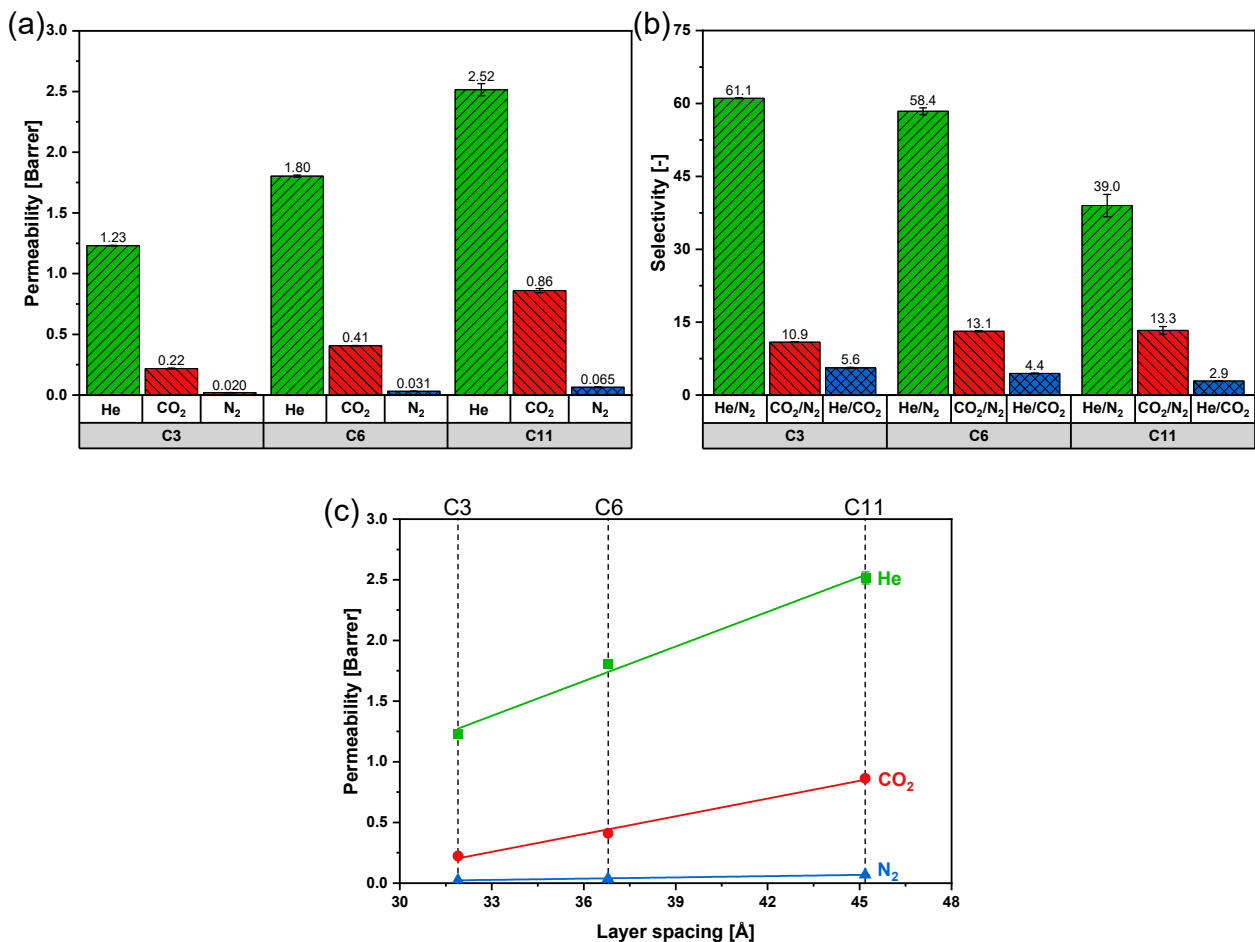


Figure 3. Gas permeation data and ideal gas selectivities of smectic LC membranes with various layer spacings. (a) Single gas permeability (He, CO₂ and N₂) of C3, C6 and C11 membranes measured at 40 °C and 6 bar feed pressure. (b) Ideal gas selectivities (He/N₂, CO₂/N₂ and He/CO₂) of C3, C6 and C11 membranes measured at 40 °C and 6 bar feed pressure. (c) Single gas permeability (He, CO₂ and N₂) versus the layer spacing of the C3, C6 and C11 membranes. The small error bars represent the spread of two independently prepared membranes, where each membrane is measured in triplicate.

Figure 3a clearly shows that the gas permeability increases with increasing alkyl spacer length, resulting in the lowest gas permeabilities for the C3 membranes and the highest gas permeabilities for the C11 membranes. Obviously, He has the highest permeability of all membranes, followed by CO₂ and N₂. As the gas permeability through dense membranes depends on the kinetic diameter and critical temperature of the gas species (see Table S4 for the kinetic diameter and critical temperature of He, CO₂ and N₂) [37]. Helium has the smallest kinetic diameter of all measured gasses, which results in a higher diffusion rate through the membrane and the highest permeability of all gasses. Contrary, N₂ has the largest kinetic diameter of all measured gasses, leading to a lower diffusion rate through the membrane. Together with a low critical temperature, which affects the condensability of a gas and thereby the solubility in the polymer matrix, this results in the lowest permeability of all measured gasses. CO₂ has a kinetic diameter between He and N₂ but has the highest critical temperature of all measured gasses, resulting in a higher solubility and permeability between He and N₂. Figure 3c shows the relation between layer spacing and gas permeability of smectic LC membranes. The permeability of all gasses decreases with decreasing layer spacing, resulting in the lowest permeabilities for the C3 membranes with a layer spacing of 31.9 Å, followed by the C6 and C11 membranes with layer spacings of, respectively, 36.8 Å and 45.2 Å. This correlation between layer spacing and gas permeability likely arises due to a change in the total free volume within the membrane or/and a change in the size of the free volume elements within the membrane upon a change in layer spacing [30]. A change in the free volume or size of the free volume elements within dense membranes affects the solubility and diffusion of gasses, which can lead to different gas permeabilities. Contrary to the permeability, the ideal gas selectivity of He/N₂ and He/CO₂ decreases with increasing layer spacing (Figure 3b), resulting in the highest selectivities for the C3 membranes (respectively 61.1 for He/N₂ and 5.6 for He/CO₂) and the lowest selectivities for the C11 membranes (respectively 39.0 for He/N₂ and 2.9 for He/CO₂). The decrease in selectivity towards He probably originates from the increasing layer spacing of the lamellar structures, which results in larger free volume elements within the membrane. This affects the diffusion of gasses with larger kinetic diameters such as CO₂ and N₂ more compared to the smaller He, resulting in a lower selectivity towards He. As the separation of He/N₂ and He/CO₂ gas pairs are mainly diffusion-controlled, the selectivities decrease with increasing layer spacing of the lamellar structures. The CO₂/N₂ selectivity of the C6 and C11 membranes is similar, but the CO₂/N₂ selectivity of the C3 membranes is surprisingly lower compared to the C6 and C11 membranes. Similar CO₂/N₂ selectivities were expected because the difference in kinetic diameter of CO₂ and N₂ (3.30 Å for CO₂ and 3.64 Å for N₂) is smaller compared to the difference in kinetic diameter of He and N₂ (2.60 Å for He and 3.64 Å for N₂), resulting in comparable diffusion rates of CO₂ and N₂ through the membrane. Moreover, the separation of the CO₂/N₂ gas pair is mainly sorption-controlled, meaning that these gasses are mainly separated by their differences in gas solubility rather than differences in diffusion. This reduces the influence of the layer spacing on the permeability of CO₂ and N₂ and leads to very similar CO₂/N₂ selectivities for the C6 and C11 membranes.

3.4. Effect of Halogenation on Single Gas Performances

The effect of halogenation on the gas separation properties of smectic LC membranes was investigated by measuring the single gas permeation of He, CO₂ and N₂ at 40 °C for C6 membranes with various halogenated LCs (respectively 30 wt% C6-Cl₁, 30 wt% C6-Cl₂ and 25 wt% C6-F₄). The permeation data and ideal gas selectivities of He/N₂, CO₂/N₂ and He/CO₂ are shown in Figure 4 (see Tables S5 and S6 for permeation and ideal selectivity values). For comparison, and to show the effect of halogenation in more detail, the permeation and ideal selectivity data of the C6 membranes without halogenated LCs are also included in Figure 4.

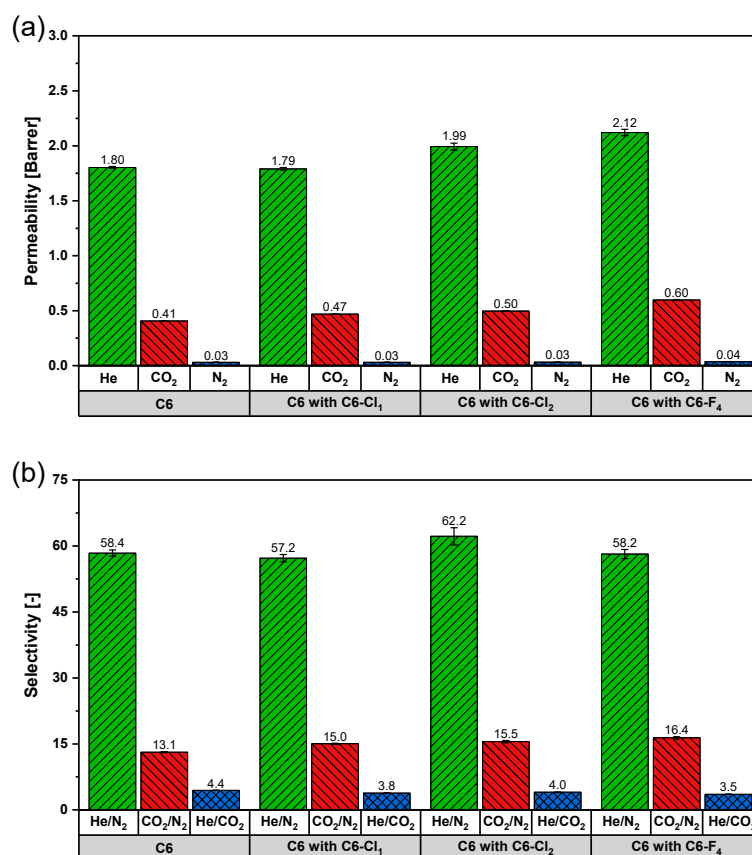


Figure 4. Gas permeation data and ideal gas selectivities of smectic LC membranes with various halogenated LCs. (a) Single gas permeability (He, CO₂ and N₂) of smectic C6 membranes with respectively 30 wt% C6-Cl₁, 30 wt% C6-Cl₂ and 25 wt% C6-F₄ measured at 40 °C and 6 bar feed pressure. (b) Ideal gas selectivities (He/N₂, CO₂/N₂ and He/CO₂) of smectic C6 membranes with respectively 30 wt% C6-Cl₁, 30 wt% C6-Cl₂ and 25 wt% C6-F₄ at 40 °C. The small error bars represent the spread of two independently prepared membranes, where each membrane is measured in triplicate.

Figure 4a shows that the C6 membranes with halogenated LCs only exhibit slightly higher permeabilities compared to the C6 membranes without halogenated LCs. These small differences likely arise from the relatively low halogen content in the halogenated C6 membranes (30 wt% for the membranes with C6-Cl₁ and C6-Cl₂ and 25 wt% for the membranes with C6-F₄), which is needed to obtain a smectic morphology. Despite the small permeability differences, the membranes show some subtle variations in permeation behavior. The permeability of all gasses increases with increasing halogen content, resulting in the highest permeabilities for the membranes with 25 wt% C6-F₄. The membranes with 30 wt% C6-Cl₁ only show an increase in CO₂ permeability, while the membranes with C6-Cl₂ and C6-F₄ show increased permeabilities for all gasses. The increased permeabilities for the membranes with halogenated LCs likely arises due to an increase in the total free volume and/or size of the free volume elements within the membranes with increasing halogen content. The bulky halogen substituents disrupt the chain packing of the molecules, which increases the diffusion coefficient of all gasses, resulting in higher gas permeabilities for the membranes with halogenated LCs compared to the pristine C6 membranes. The CO₂ permeability of all membranes shows a relatively larger permeability increase compared to He and N₂. This can be explained two-fold. Firstly, the quadrupole of CO₂ interacts favorably with the polar halogen groups, which leads to a higher solubility in the polymer matrix and therefore to a higher CO₂ permeability (Table S3 for quadrupole moments of He, CO₂ and N₂). Gasses without these favorable interactions (He) or gasses with only small interactions (N₂) are less affected by the polarity of the halogen groups, resulting in a lower permeability increase [29–31]. Secondly, C6 membranes that contain halogenated LCs

show slightly higher layer spacings compared to the C6 membranes without halogenated LCs, which also affect the diffusion of gasses through the membranes and lead to an increase in permeability (see Sections 3.2 and 3.3). Contrary to the membranes with various alkyl spacer lengths, Figure 4b shows that the He/N₂ selectivity of the C6 membranes with halogenated LCs is similar for all membranes. Here, the small increase in layer spacing with increasing halogen content does not affect the selectivity towards He. The selectivity towards CO₂ increases with increasing halogen content due to improved CO₂-polymer matrix interactions, resulting in higher CO₂/N₂ selectivities and lower He/CO₂ selectivities for the C6 membranes with halogenated LCs compared to the C6 membranes. These permeation results show that the used halogen content, which is necessary to obtain smectic LC membranes, only has a limited effect on the gas separation performances (permeability/selectivity) of smectic LC membranes.

3.5. CO₂ Sorption

Since the gas permeability of dense membranes is defined as the product of the solubility coefficient and the diffusion coefficient of a certain gas species, CO₂ sorption was measured to determine the CO₂ solubility coefficient and further investigate the effect of layer spacing and halogenation on gas solubility and diffusion in smectic LC membranes. The diffusion coefficient was subsequently calculated using Equation (6). Unfortunately, only CO₂ sorption could be measured because the N₂ sorption was for all membranes too low to obtain accurate values. The layer spacing, CO₂ permeabilities, CO₂ solubility coefficients and the associated calculated diffusion coefficients of all membranes are shown in Table 4. To illustrate the effect of the layer spacing in more detail, the solubility coefficients and the diffusion coefficients were also plotted against the layer spacing of the membranes (Figure 5).

Table 4. The layer spacing, CO₂ permeabilities, CO₂ solubility coefficients measured at 40 °C and 6 bar and the associated calculated diffusion coefficients of all membranes.

Membrane	Layer Spacing [Å]	$\frac{P}{\left[\frac{\text{cm}^3(\text{STP}) \cdot \text{cm}}{\text{cm}^2 \cdot \text{s} \cdot \text{cmHg}}\right]} \cdot 10^{-10}$	$\frac{S}{\left[\frac{\text{cm}^3(\text{STP})}{\text{cm}^3 \cdot \text{cmHg}}\right]} \cdot 10^{-3}$	$\frac{D}{\left[\frac{\text{cm}^2}{\text{s}}\right]} \cdot 10^{-9}$
C3	31.9	0.22	6.94	3.16
C6	36.8	0.41	5.95	6.85
C11	45.2	0.86	4.68	18.37
C6 with 30 wt% C6-Cl ₁	37.4	0.47	5.86	8.01
C6 with 30 wt% C6-Cl ₂	37.5	0.50	6.05	8.22
C6 with 25 wt% C6-F ₄	38.1	0.60	6.74	8.88

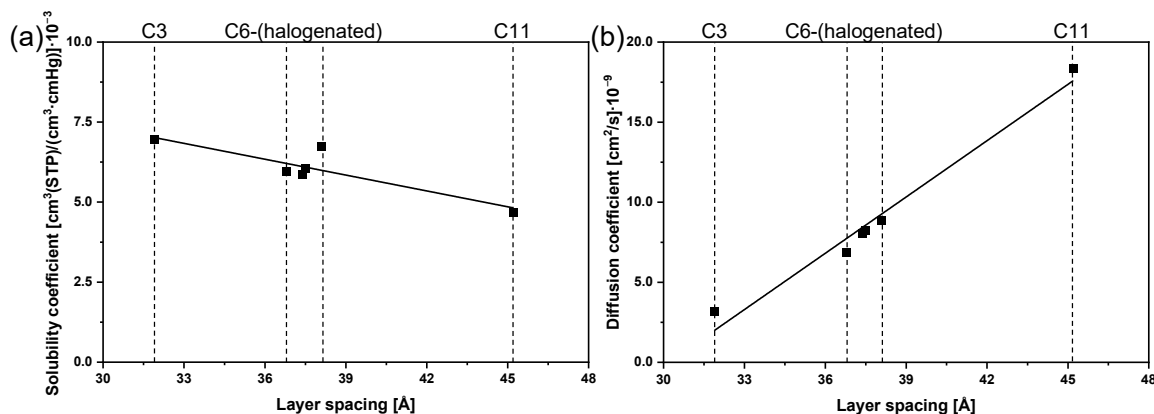


Figure 5. Effect of layer spacing on the CO₂ (a) solubility coefficient (b) and diffusion coefficient in smectic LC membranes.

Sorption experiments in Table 4 show that the layer spacing affects both the CO₂ solubility coefficients and the diffusion coefficients of smectic LC membranes. The solubility coefficients slightly decrease with increasing layer spacing (Figure 5a), resulting in the highest solubility coefficient for the C3 membranes and the lowest solubility coefficient for the C11 membranes. This decrease in solubility coefficient with increasing layer spacing can be explained as follows. Varying the alkyl spacer length of the LC monomers not only affects the layer spacing but also the amount of ether/ester groups present in the membrane. The polar ether/ester oxygen groups interact favorably with the quadrupole of CO₂, which usually leads to higher CO₂ solubility coefficients for the membranes with more ether/ester groups [38–42]. The ether/ester content of the membranes decreases with increasing alkyl spacer length, resulting in the highest CO₂ solubility coefficient for the C3 membranes and lower CO₂ solubility coefficients for the C6 and C11 membranes (C3 > C6 > C11). Furthermore, the C6 membranes with halogenated LCs show slightly higher solubility coefficients compared to the C6 membranes, showing the highest solubility coefficient for the C6 membranes with 25 wt% C6-F₄. Here, additional favorable interactions between CO₂ and the polar halogen groups lead to improved CO₂-polymer matrix interactions, which results in a higher solubility coefficient with increasing halogen content. Contrary to the solubility coefficient, the diffusion coefficient increases tremendously with increasing layer spacing (Figure 5b). The diffusion coefficient of the C6 membranes is 2 times higher compared to the C3 membranes, while the C11 membranes even show a 6-fold increase in the diffusion coefficient compared to the C3 membranes. This indicates that the increasing gas permeability with increasing layer spacing for the C3, C6 and C11 membranes can be attributed to an increasing diffusion coefficient. However, the aromatic-aliphatic ratio, which is increasing when going from C11 to C3, might also affect the diffusion coefficient. For the C6 membranes with halogenated LCs, the slight increase in CO₂ permeability and selectivity can be attributed to an increase in both solubility and diffusion coefficients. The bulky polar halogen groups in the halogenated C6 membranes lead to improved CO₂-polymer matrix interactions and slightly higher layer spacing values, resulting in increased solubility and diffusion coefficients for the C6 membranes with halogenated LCs compared to the C6 membranes without halogenated LCs.

The solubility and diffusion coefficients of gasses are highly affected by the available free volume and the size of the free volume elements within the membrane. Usually, both the solubility and diffusion coefficients increase with increasing free volume within a membrane because higher amounts of the free volume provide more sorption sites for gasses. Next to the overall free volume, the diffusion coefficient is also affected by the size of the free volume elements. The activation energy of diffusion is lower for larger free volume elements leading, to a higher diffusion coefficient. The very similar solubility coefficients for all membranes indicate that the overall free volume is equal and is not much affected by either the layer spacing or the bulky polar halogen groups in the smectic structures [43]. It is therefore expected that with increasing layer spacing, not the total free volume within the smectic LC membrane increases, but the free volume elements within the membrane increase in size. This increases the diffusion coefficients for all gasses, leading to higher permeabilities with increasing layer spacing values. However, the diffusion coefficient of gasses with larger kinetic diameters (CO₂ and N₂) is more affected by the size of the free volume elements compared to gasses with a smaller kinetic diameter (He), resulting in lower selectivities towards He for the C11 membranes [44,45].

4. Conclusions

The effects of the layer spacing and halogenation on the gas separation performance of free-standing planar aligned smectic LC polymer membranes for gas separations of He, CO₂ and N₂ were investigated. All LC membranes consisting of LCs with similar chemical compositions but different alkyl spacer lengths and membranes containing halogenated LCs have a planar alignment and smectic morphology. The tilt angle of the smectic structures was similar for all membranes, but the layer spacing was found to be highly dependent

on the length of the alkyl spacer, resulting in smectic LC membranes with various layer spacing values.

Gas sorption of CO₂ and single gas permeation of He, CO₂ and N₂ demonstrated that the permeability increases with increasing layer spacing, while the ideal gas selectivity towards He decreases with increasing layer spacing. It was found that an increasing diffusion coefficient with increasing layer spacing is responsible for the increased permeability, showing that the layer spacing in smectic LC membranes mainly affects the diffusion of gasses rather than their solubility. The effect of incorporating bulky halogens onto the LC cores has been shown to only have a limited effect on the gas permeability and ideal gas selectivity due to the relatively low halogen content in the used membranes, which was needed to maintain a smectic morphology. The CO₂ permeability of all membranes with halogenated LCs slightly increases with increasing halogen content due to an increase in CO₂ solubility and diffusion coefficients, resulting in slightly improved selectivities towards CO₂.

Our results show that especially layer spacing is a crucial parameter that directly controls the diffusion coefficient of gasses in smectic LC membranes and can be used to tune their gas separation performances (permeability/selectivity). Future work should focus on improving the separation performances by reducing the membrane thickness. This research provides insights into the structure-performance relations with single gas measurements, but future research should study the performances under mixed-gas conditions and investigate plasticization and physical aging of the membranes.

Supplementary Materials: The following supporting information can be downloaded at: <https://www.mdpi.com/article/10.3390/membranes12080805/s1>, The synthetic procedures to prepare compounds **C3**, **C6-Cl₁** and **C6-Cl₂** and characterizations of these compounds; Figures S1–S9: DSC and POM images of the compounds and mixtures of **C3**, **C6**, **C11**, **C6-Cl₁**, **C6-Cl₂** and **C6-F₄**; Figure S10: FT-IR of **C6** before and after polymerization; Figure S11: POM images of the prepared membranes; Table S1: Phase transitions of the used LC mixtures.; Table S2: Permeabilities of LC membranes with various layer spacings; Table S3: Ideal gas selectivities of LC membranes with various layer spacings; Table S4: Kinetic diameter, critical temperature and quadrupole moment of He, CO₂ and N₂; Table S5: Permeabilities of LC membranes with halogenated LCs; Table S6: Ideal gas selectivities of LC membranes with halogenated LCs.

Author Contributions: J.K.: conceptualization, methodology, validation, formal analysis, investigation, writing—original draft, writing—review and editing, visualization. M.H.: formal analysis, investigation, writing—review and editing. J.L.: formal analysis, investigation, writing—review and editing. K.N.: conceptualization, supervision, writing—review and editing, project administration, funding acquisition. A.P.H.J.S.: conceptualization, writing—review and editing. Z.B.: conceptualization, supervision, writing—review and editing. All authors have read and agreed to the published version of the manuscript.

Funding: This research was part of the research program START-UP with project number 740.018.005, which is financed by the Dutch Organization for Scientific Research (NWO).

Institutional Review Board Statement: Not applicable.

Informed Consent Statement: Not applicable.

Acknowledgments: The authors want to thank Anna Casimiro of the Eindhoven University of Technology for her help with the MAXS/WAXS measurements, Lou Xianwen of the Eindhoven University of Technology for his help with MALDI-TOF measurements and Mariola Cervera of the Zaragoza University for making one of the batches of 4-(3-acryloyloxypropyloxy)phenyl 4-(4-(3-acryloyloxypropyloxy)benzoyloxy)benzoate (compound **C3**).

Conflicts of Interest: The authors declare no conflict of interest.

References

1. Huang, L.; Liu, J.; Lin, H. Thermally Stable, Homogeneous Blends of Cross-Linked Poly(Ethylene Oxide) and Crown Ethers with Enhanced CO₂ Permeability. *J. Memb. Sci.* **2020**, *610*, 118253. [[CrossRef](#)]
2. Wang, S.; Li, X.; Wu, H.; Tian, Z.; Xin, Q.; He, G.; Peng, D.; Chen, S.; Yin, Y.; Jiang, Z.; et al. Advances in High Permeability Polymer-Based Membrane Materials for CO₂ Separations. *Energy Environ. Sci.* **2016**, *9*, 1863–1890. [[CrossRef](#)]
3. Basu, S.; Khan, A.L.; Cano-Odena, A.; Liu, C.; Vankelecom, I.F.J. Membrane-Based Technologies for Biogas Separations. *Chem. Soc. Rev.* **2010**, *39*, 750–768. [[CrossRef](#)]
4. Bernardo, P.; Drioli, E.; Golemme, G. Membrane Gas Separation: A Review/State of the Art. *Ind. Eng. Chem. Res.* **2009**, *48*, 4638–4663. [[CrossRef](#)]
5. Sanders, D.F.; Smith, Z.P.; Guo, R.; Robeson, L.M.; McGrath, J.E.; Paul, D.R.; Freeman, B.D. Energy-Efficient Polymeric Gas Separation Membranes for a Sustainable Future: A Review. *Polymer* **2013**, *54*, 4729–4761. [[CrossRef](#)]
6. Rufford, T.E.; Smart, S.; Watson, G.C.Y.; Graham, B.F.; Boxall, J.; Diniz da Costa, J.C.; May, E.F. The Removal of CO₂ and N₂ from Natural Gas: A Review of Conventional and Emerging Process Technologies. *J. Pet. Sci. Eng.* **2012**, *94–95*, 123–154. [[CrossRef](#)]
7. Kim, S.; Lee, Y.M. High Performance Polymer Membranes for CO₂ Separation. *Curr. Opin. Chem. Eng.* **2013**, *2*, 238–244. [[CrossRef](#)]
8. Hamid, M.R.A.; Jeong, H.K. Recent Advances on Mixed-Matrix Membranes for Gas Separation: Opportunities and Engineering Challenges. *Korean J. Chem. Eng.* **2018**, *35*, 1577–1600. [[CrossRef](#)]
9. Sridhar, S.; Smitha, B.; Aminabhavi, T.M. Separation of Carbon Dioxide from Natural Gas Mixtures through Polymeric Membranes—A Review. *Sep. Purif. Rev.* **2007**, *36*, 113–174. [[CrossRef](#)]
10. Freeman, B.D. Basis of Permeability/Selectivity Tradeoff Relations in Polymeric Gas Separation Membranes. *Macromolecules* **1999**, *32*, 375–380. [[CrossRef](#)]
11. Burns, R.L.; Steel, K.M.; Burns, S.D.; Koros, W.J. Explanation of a Selectivity Maximum, as a Function of the Material Structure for Organic Gas Separation Membranes. *Ind. Eng. Chem. Res.* **2004**, *43*, 5942–5949. [[CrossRef](#)]
12. Robeson, L.M. The Upper Bound Revisited. *J. Memb. Sci.* **2008**, *320*, 390–400. [[CrossRef](#)]
13. Zhou, M.; Kidd, T.J.; Noble, R.D.; Gin, D.L. Supported Lyotropic Liquid-Crystal Polymer Membranes: Promising Materials for Molecular-Size-Selective Aqueous Nanofiltration. *Adv. Mater.* **2005**, *17*, 1850–1853. [[CrossRef](#)]
14. Bögels, G.M.; Lugger, J.A.M.; Goor, O.J.G.M.; Sijbesma, R.P. Size-Selective Binding of Sodium and Potassium Ions in Nanoporous Thin Films of Polymerized Liquid Crystals. *Adv. Funct. Mater.* **2016**, *26*, 8023–8030. [[CrossRef](#)]
15. Dischinger, S.M.; Rosenblum, J.; Noble, R.D.; Gin, D.L.; Linden, K.G. Application of a Lyotropic Liquid Crystal Nano Filtration Membrane for Hydraulic Fracturing Flowback Water: Selectivity and Implications for Treatment. *J. Memb. Sci.* **2017**, *543*, 319–327. [[CrossRef](#)]
16. Marets, N.; Kuo, D.; Torrey, J.R.; Sakamoto, T.; Henmi, M.; Katayama, H.; Kato, T. Highly Efficient Virus Rejection with Self-Organized Membranes Based on a Crosslinked Bicontinuous Cubic Liquid Crystal. *Adv. Healthc. Mater.* **2017**, *6*, 1700252. [[CrossRef](#)] [[PubMed](#)]
17. Henmi, M.; Nakatsuji, K.; Ichikawa, T.; Tomioka, H.; Sakamoto, T.; Yoshio, M.; Kato, T. Self-Organized Liquid-Crystalline Nanostructured Membranes for Water Treatment: Selective Permeation of Ions. *Adv. Mater.* **2012**, *24*, 2238–2241. [[CrossRef](#)]
18. Sasaki, T.; Hazato, H.; Katsuragi, A.; Nakazawa, Y. Photorefractive Effect of Photoconductive-Polymer-Stabilized Ferroelectric Liquid Crystals. *Mol. Cryst. Liq. Cryst.* **2009**, *503*, 81–98. [[CrossRef](#)]
19. Li, C.; Cho, J.; Yamada, K.; Hashizume, D.; Araoka, F.; Takezoe, H.; Aida, T.; Ishida, Y. Macroscopic Ordering of Helical Pores for Arraying Guest Molecules Noncentrosymmetrically. *Nat. Commun.* **2015**, *6*, 8418. [[CrossRef](#)]
20. Gupta, M.; Suzuki, Y.; Sakamoto, T.; Yoshio, M.; Torii, S.; Katayama, H.; Kato, T. Polymerizable Photocleavable Columnar Liquid Crystals for Nanoporous Water Treatment Membranes. *ACS Macro Lett.* **2019**, *8*, 1303–1308. [[CrossRef](#)]
21. Sakamoto, T.; Ogawa, T.; Nada, H.; Nakatsuji, K.; Mitani, M.; Soberats, B.; Kawata, K.; Yoshio, M.; Tomioka, H.; Sasaki, T.; et al. Development of Nanostructured Water Treatment Membranes Based on Thermotropic Liquid Crystals: Molecular Design of Sub-Nanoporous Materials. *Adv. Sci.* **2018**, *5*, 1700405. [[CrossRef](#)] [[PubMed](#)]
22. Van Kuringen, H.P.C.; Eikelboom, G.M.; Shishmanova, I.K.; Broer, D.J.; Schenning, A.P.H.J. Responsive Nanoporous Smectic Liquid Crystal Polymer Networks as Efficient and Selective Adsorbents. *Adv. Funct. Mater.* **2014**, *24*, 5045–5051. [[CrossRef](#)]
23. Liang, T.; Van Kuringen, H.P.C.; Mulder, D.J.; Tan, S.; Wu, Y.; Borneman, Z.; Nijmeijer, K.; Schenning, A.P.H.J. Anisotropic Dye Adsorption and Anhydrous Proton Conductivity in Smectic Liquid Crystal Networks: The Role of Cross-Link Density, Order, and Orientation. *ACS Appl. Mater. Interfaces* **2017**, *9*, 35218–35225. [[CrossRef](#)] [[PubMed](#)]
24. Zhou, M.; Nemade, P.R.; Lu, X.; Zeng, X.; Hatakeyama, E.S.; Noble, R.D.; Gin, D.L. New Type of Membrane Material for Water Desalination Based on a Cross-Linked Bicontinuous Cubic Lyotropic Liquid Crystal Assembly. *J. Am. Chem. Soc.* **2007**, *129*, 9574–9575. [[CrossRef](#)]
25. Bara, J.E.; Kaminski, A.K.; Noble, R.D.; Gin, D.L. Influence of Nanostructure on Light Gas Separations in Cross-Linked Lyotropic Liquid Crystal Membranes. *J. Memb. Sci.* **2007**, *288*, 13–19. [[CrossRef](#)]
26. Kloos, J.; Jansen, N.; Houben, M.; Casimiro, A.; Lub, J.; Borneman, Z.; Schenning, A.P.H.J.; Nijmeijer, K. On the Order and Orientation in Liquid Crystalline Polymer Membranes for Gas Separation. *Chem. Mater.* **2021**, *33*, 8323–8333. [[CrossRef](#)]
27. Houben, S.J.A.; Kloos, J.; Borneman, Z.; Schenning, A.P.H.J. Switchable Gas Permeability of a Polypropylene-Liquid Crystalline Composite Film. *J. Polym. Sci.* **2022**, *60*, 803–811. [[CrossRef](#)]

28. Kloos, J.; Jansen, N.; Houben, M.; Nijmeijer, K.; Schenning, A.P.H.J.; Borneman, Z. Molecular Order Determines Gas Transport through Smectic Liquid Crystalline Polymer Membranes with Different Chemical Compositions. *ACS Appl. Polym. Mater.* *submitt.*
29. Ghosal, K.; Freeman, B.D. Gas Separation Using Polymer Membranes: An Overview. *Polym. Adv. Technol.* **1994**, *5*, 673–697. [[CrossRef](#)]
30. Hellums, M.W.; Koros, W.J.; Husk, G.R.; Paul, D.R. Fluorinated Polycarbonates for Gas Separation Applications. *J. Memb. Sci.* **1989**, *46*, 93–112. [[CrossRef](#)]
31. Wang, X.; Wilson, T.J.; Maroon, C.R.; Laub, J.A.; Rheingold, S.E.; Vogiatzis, K.D.; Long, B.K. Vinyl-Addition Fluoroalkoxysilyl-Substituted Polynorbornene Membranes for CO₂/CH₄ Separation. *ACS Appl. Polym. Mater.* **2022**. [[CrossRef](#)]
32. Kadir Khan, F.; Goh, P.S.; Ismail, A.F.; Wan Mustapa, W.N.F.; Halim, M.H.M.; Soh, W.K.; Yeo, S.Y. Recent Advances of Polymeric Membranes in Tackling Plasticization and Aging for Practical Industrial CO₂/CH₄ Applications—A Review. *Membranes* **2022**, *12*, 71. [[CrossRef](#)] [[PubMed](#)]
33. Hikmet, R.A.M.; Lub, J.; Tol, A.J.W. Effect of the Orientation of the Ester Bonds on the Properties of Three Isomeric Liquid Crystal Diacrylates before and after Polymerization. *Macromolecules* **1995**, *28*, 3313–3327. [[CrossRef](#)]
34. Ikenaga, M.; Kubota, D.; Yamamoto, T. Liquid Crystal Composition, Liquid Crystal Element, and Liquid Crystals Display Device. U.S. Patent 2013/0256595 A1, 3 October 2013.
35. Dallacker, F.; van Wersch, J. Synthese von Apiolanaloga, II. *Chem. Ber.* **1972**, *105*, 3301–3305. [[CrossRef](#)]
36. Sikirić, M.; Primožič, I.; Talmon, Y.; Filipović-Vinceković, N. Effect of the Spacer Length on the Association and Adsorption Behavior of Dissymmetric Gemini Surfactants. *J. Colloid Interface Sci.* **2005**, *281*, 473–481. [[CrossRef](#)] [[PubMed](#)]
37. Rallapalli, P.; Prasanth, K.P.; Patil, D.; Somani, R.S.; Jasra, R.V.; Bajaj, H.C. Sorption Studies of CO₂, CH₄, N₂, CO, O₂ and Ar on Nanoporous Aluminum Terephthalate [MIL-53(Al)]. *J. Porous Mater.* **2011**, *18*, 205–210. [[CrossRef](#)]
38. Houben, M.; Borneman, Z.; Nijmeijer, K. Plasticization Behavior of Crown-Ether Containing Polyimide Membranes for the Separation of CO₂. *Sep. Purif. Technol.* **2021**, *255*, 117307. [[CrossRef](#)]
39. Reijerkerk, S.R.; Arun, A.; Gaymans, R.J.; Nijmeijer, K.; Wessling, M. Tuning of Mass Transport Properties of Multi-Block Copolymers for CO₂ Capture Applications. *J. Memb. Sci.* **2010**, *359*, 54–63. [[CrossRef](#)]
40. Car, A.; Stropnik, C.; Yave, W.; Peinemann, K.V. Pebax®/Polyethylene Glycol Blend Thin Film Composite Membranes for CO₂ Separation: Performance with Mixed Gases. *Sep. Purif. Technol.* **2008**, *62*, 110–117. [[CrossRef](#)]
41. Chen, H.Z.; Chung, T.S. CO₂-Selective Membranes for Hydrogen Purification and the Effect of Carbon Monoxide (CO) on Its Gas Separation Performance. *Int. J. Hydrogen Energy* **2012**, *37*, 6001–6011. [[CrossRef](#)]
42. Liu, J.; Zhang, G.; Clark, K.; Lin, H. Maximizing Ether Oxygen Content in Polymers for Membrane CO₂ Removal from Natural Gas. *ACS Appl. Mater. Interfaces* **2019**, *11*, 10933–10940. [[CrossRef](#)]
43. Hu, C.C.; Chang, C.S.; Ruaan, R.C.; Lai, J.Y. Effect of Free Volume and Sorption on Membrane Gas Transport. *J. Memb. Sci.* **2003**, *226*, 51–61. [[CrossRef](#)]
44. Haraya, K.; Hwang, S.T. Permeation of Oxygen, Argon and Nitrogen through Polymer Membranes. *J. Memb. Sci.* **1992**, *71*, 13–27. [[CrossRef](#)]
45. Thornton, A.W.; Nairn, K.M.; Hill, A.J.; Hill, J.M. New Relation between Diffusion and Free Volume: I. Predicting Gas Diffusion. *J. Memb. Sci.* **2009**, *338*, 29–37. [[CrossRef](#)]